Bioorganic Chemistry 93 (2019) 103303

Contents lists available at ScienceDirect

Bioorganic Chemistry

journal homepage: www.elsevier.com/locate/bioorg

Chiral resolution of a caged xanthone and evaluation across a broad spectrum of breast cancer subtypes

Oraphin Chantarasriwong[a,b], Tanis J. Dorwart[c], Theodore Habarth Morales[c], Stephanie F. Maggio[c], Aspen L. Settle[c], Andrew T. Milcarek[d], Mary L. Alpaugh[d,*], Maria A. Theodoraki[c,*], Emmanuel A. Theodorakis[a,*]

[a] Department of Chemistry and Biochemistry, University of California, San Diego, 9500 Gilman Drive, La Jolla, CA 92093-0358, USA
[b] Department of Chemistry, Faculty of Science, King Mongkut's University of Technology Thonburi, 126 Pracha Uthit Rd., Bang Mod, Thung Khru, Bangkok 10140, Thailand
[c] Department of Biology, Arcadia University, Glenside, PA 19038, USA
[d] Department of Molecular and Cellular Biosciences, Rowan University, Glassboro, NJ 08028, USA

ARTICLE INFO

Keywords:
Natural product
Synthetic methods
Garcinia
Gambogic acid
Breast cancer

ABSTRACT

Racemic resolution of **(+/−)-MAD28**, a representative caged xanthone, was accomplished using (1S, 4R)-(−)-camphanic chloride as the chiral agent. Selective crystallization of the resulting diastereomers in acetonitrile produced, after hydrolysis, the pure enantiomers. Screening of racemic **MAD28** and both enantiomers across a broad spectrum of breast cancer cell lines revealed that they: (a) are equipotent in each of the breast cancer subtypes examined; and (b) exhibit a higher degree of cytotoxicity against breast cancer cell lines of basal-like subtype and triple negative receptor status. The results support the notion that **MAD28** and related caged xanthones are promising drug leads against chemoresistant and metastatic cancers.

1. Introduction

Isolated mainly from plants of the *Garcinia* genus, caged xanthones (CXs) [1–3], exhibit a broad spectrum of bioactivities as antibacterial, antiviral, anticancer and antimalarial agents [4–11]. Their therapeutic potential is highlighted by gambogic acid (**GBA**, **1**) [12–17] (Fig. 1), the archetype of this family, that has entered clinical trials in China as an anticancer agent [18,19]. In terms of chemical structure, **GBA** contains a unique caged structure at the C-ring of a xanthone scaffold that is encountered in all members of this family. In terms of biological mode of action, **GBA** was found to interfere with several protein targets such as the proteasome [20,21], topoisomerase II [22], Bcl-2 [23,24] and the heat shock protein Hsp90 [25–28]. In cancer cells, these interactions lead to mitochondrial toxicity and cell death in a tissue-selective manner [29–34]. Structure-activity relationship studies identified cluvenone (**CLV**, 2), a synthetic CX analogue containing the C-ring caged motif as the pharmacophoric motif of this family (blue scaffold in Fig. 1) [35,36]. Moreover, installation of a hydroxyl group at the C6 position resulted in compound **MAD28** (**3**) that exerts significantly improved cytotoxicity against a variety of cancer cell lines [26,37–41]. Recently, **MAD28** was found to exhibit potent cytotoxicity in a 3-dimensional (3D) *in vitro* model of inflammatory breast cancer [42,43], a unique subtype of breast cancer with a drug-resistant and highly metastatic phenotype [44–47]. These findings suggest that **MAD28** can serve as a starting point for the development of drugs against chemoresistant cancers for which there is no efficient pharmacological treatment [48,49].

By virtue of their biosynthesis, caged xanthones are usually isolated either as racemates or as scalemic mixtures of low enantiomeric excess [50–55]. Consequently, most of the biological studies have been performed with mixtures of variable or undetermined enantiomeric composition. Efforts to separate enantiomerically pure compounds have relied mainly on chiral HPLC purification that is not readily amenable to large-scale purification [52–54]. This challenge can be addressed using chiral resolution techniques that, to the best of our knowledge, have not been explored [5,6]. Here we report such a method to resolve **(+/−)-MAD28**, a representative CX, using camphanic chloride as a chiral resolving agent. This approach is amenable to scale-up and could be used to separate other synthetic or natural members of the CX family. In addition, we evaluated the activity of racemic **MAD28** and its enantiomers across a broad spectrum of breast cancer subtypes. The enantiomers were found to be equipotent in each of the molecularly-

* Corresponding authors.
E-mail addresses: alpaugh@rowan.edu (M.L. Alpaugh), theodorakim@arcadia.edu (M.A. Theodoraki), etheodorakis@ucsd.edu (E.A. Theodorakis).

https://doi.org/10.1016/j.bioorg.2019.103303
Received 8 July 2019; Received in revised form 15 August 2019; Accepted 17 September 2019
Available online 21 September 2019

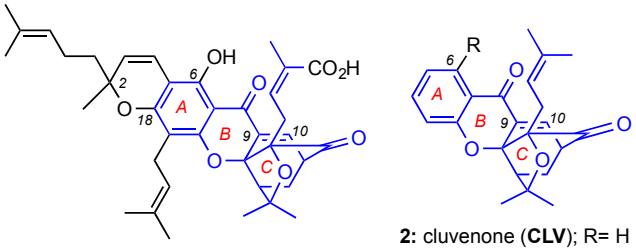

Fig. 1. Chemical structures of gambogic acid (**GBA**), cluvenone (**CLV**) and hydroxylated analogue **MAD28**.

defined breast cancer subtypes. Additionally, they exhibited approximately 2-fold higher degree of efficacy (1.6 μM IC_{50} vs. 3.5 μM IC_{50}) between the basal vs. the human epithelial growth factor receptor 2 (HER2) enriched and luminal B subtypes, respectively.

2. Experimental section

2.1. General experimental procedures

(1*S*, 4*R*)-(−)-camphanic chloride was purchased from Sigma-Aldrich (> 96.0%, $[\alpha]_D^{23}$ = –18, *c* = 2.0, CCl_4). $Pd(PPh_3)_4$ was purchased from Strem Chemicals, Inc. (Newburyport, MA). The rest of the reagents were obtained (Sigma-Aldrich, Acros) at highest commercial quality and used without further purification except where noted. All nonaqueous reactions were carried out under argon atmosphere using dry glassware that had been flame-dried under a stream of argon unless otherwise noted. Anhydrous tetrahydrofuran (THF) and dimethylformamide (DMF) were obtained by passing commercially available pre-dried, oxygen-free formulations through activated alumina columns. Flash column chromatography was performed on silica gel (Merck Kieselgel 60, 230–400 mesh). The progress of all the reactions was monitored by thin-layer chromatography (TLC) using glass plates precoated with silica gel-60 F254 to a thickness of 0.5 mm (Merck), and compounds were visualized by irradiation with UV light and/or by treatment with a solution of CAM or $KMnO_4$ stain followed by heating. ^{1}H NMR and ^{13}C NMR spectra were recorded on a 400 or 500 MHz Varian or a 500 JEOL instrument. Chemical shifts (δ) are quoted in parts per million (ppm) referenced to the appropriate residual solvent peak reference ($CDCl_3$), with the abbreviations s, d, t, dd, m, denoting singlet, doublet, triplet, doublet of doublets and multiplet, respectively. *J* is a coupling constant given in Hertz (Hz). High resolution mass spectra (HRMS) were recorded on a Bruker microTOF mass spectrometer under electrospray ionization (ESI) conditions. Optical rotation data were collected on a Jasco P-1010 polarimeter using HPLC grade anhydrous $CHCl_3$. The single crystal X-ray diffraction studies were carried out on a Bruker Kappa APEX-II CCD diffractometer equipped with Cu K_α radiation (λ = 1.5478). HPLC analysis was performed on a JASCO HPLC system equipped with a UV-2075 Plus spectrometer, PU-2080 Plus pumps and an MX-2080-32 dynamic mixer using a Lux® 5 μm Amylose-2 column (250 × 4.6 mm) with detection at 250 nm using HPLC grade 50% ACN/H_2O as eluent and a flow rate of 1.2 mL/min. ECD spectra were recorded on a Jacsco J-810 spectropolarimeter in 0.2 cm quartz cell at 23 °C using HPLC grade anhydrous MeOH.

2.2. Synthetic procedures of (−)-diastereomer *8* and (+)-diastereomer *9*

To a stirred solution of racemic mixture of (±)-**MAD28** (**3**) (190 mg, 0.50 mmol, 1 equiv.) in CH_2Cl_2 (7.0 mL) was added (1*S*, 4*R*)-(−)-camphanic chloride (**7**) (108 mg, 0.50 mmol, 1 equiv.), Et_3N (0.14 mL, 1.0 mmol, 2 equiv.) and 4-DMAP (30.5 mg, 0.25 mmol, 0.5 equiv.). The reaction mixture was stirred under argon at room temperature for 2 h. (1*S*, 4*R*)-(−)-Camphanic chloride (**7**) (97.5 mg, 0.45 mmol, 0.9 equiv.), Et_3N (0.14 mL, 1.0 mmol, 2 equiv.) and 4-DMAP (30.5 mg, 0.25 mmol, 0.5 equiv.) were additionally added to the reaction mixture. The reaction mixture was stirred under argon at room temperature for another 2 h to complete the reaction. The reaction was quenched by the addition of water (3 mL) and was extracted with CH_2Cl_2 (2 × 3 mL). The combined organic layers were washed with brine, dried over Mg_2SO_4, filtered and concentrated by rotary evaporation. Acetonitrile (2 mL) was added to the crude material and the solid was collected by a vacuum filtration, washed with cold acetonitrile and dried to yield (−)-diastereomer **8** (134.4 mg, 48%) as a white solid. The mother liquid was concentrated and purified through flash column chromatography (silica, 17% to 20% EtOAc/hexane) to give (+)-diastereomer **9** (89.6 mg, 32%) as a white solid.

8: R_f = 0.19 (hexane/EtOAc = 3:1); $[\alpha]_D^{23}$ = –275.6 (*c* = 0.32, $CHCl_3$); ^{1}H NMR (500 MHz, $CDCl_3$) δ 7.52 (t, *J* = 8.4 Hz, 1H), 7.31 (d, *J* = 7.0 Hz, 1H), 7.04 (d, *J* = 8.5 Hz, 1H), 6.72 (d, *J* = 7.0 Hz, 1H), 4.42–4.39 (m, 1H), 3.49–3.47 (m, 1H), 2.72–2.62 (m, 3H), 2.52–2.46 (m, 1H), 2.44 (d, *J* = 9.5 Hz, 1H), 2.34 (dd, *J* = 13.6, 4.6 Hz, 1H), 2.02–1.97 (m, 1H), 1.81–1.75 (m, 1H), 1.71 (s, 3H), 1.44–1.41 (m, 1H), 1.37 (s, 3H), 1.30 (s, 3H), 1.20 (s, 3H), 1.17 (s, 3H), 1.16 (s, 3H), 1.08 (s, 3H); ^{13}C NMR (125 MHz, $CDCl_3$) δ 202.9, 178.2, 174.6, 165.8, 160.6, 149.5, 135.8, 135.2, 134.9, 133.7, 118.9, 117.0, 116.5, 112.5, 91.3, 90.2, 84.5, 83.5, 55.1, 54.5, 48.6, 46.8, 31.2, 30.3, 29.2, 29.1, 28.9, 25.3, 25.3, 16.9, 16.9, 16.8, 9.8; HRMS (ESI) m/e calcd for $[C_{33}H_{37}O_8]^+$ $[M+H]^+$ 561.2483, found 561.2484.

9: R_f = 0.19 (hexane/EtOAc = 3:1); $[\alpha]_D^{23}$ = +183.2 (*c* = 0.29, $CHCl_3$); ^{1}H NMR (500 MHz, $CDCl_3$) δ 7.51 (t, *J* = 8.1 Hz, 1H), 7.33 (d, *J* = 7.0 Hz, 1H), 7.03 (d, *J* = 8.4 Hz, 1H), 6.71 (d, *J* = 7.9 Hz, 1H), 4.43–4.40 (m, 1H), 3.49–3.46 (m, 1H), 2.70–2.57 (m, 3H), 2.47–2.42 (m, 2H), 2.32 (dd, *J* = 13.5, 4.5 Hz, 1H), 2.02–1.96 (m, 1H), 1.80–1.75 (m, 1H), 1.70 (s, 3H), 1.38 (s, 3H), 1.34–1.30 (m, 1H), 1.30 (s, 3H), 1.19 (s, 3H), 1.17 (s, 3H), 1.17 (s, 3H), 1.03 (s, 3H); ^{13}C NMR (125 MHz, $CDCl_3$) δ 202.9, 178.3, 174.6, 165.9, 160.7, 149.6, 135.9, 135.3, 134.8, 133.9, 118.6, 117.0, 116.5, 112.4, 91.1, 90.3, 84.5, 83.5, 55.1, 54.6, 48.7, 46.8, 31.3, 30.3, 29.1, 29.1, 28.9, 25.5, 25.2, 16.9, 16.8, 16.7, 9.8; HRMS (ESI) m/e calcd for $[C_{33}H_{37}O_8]^+$ $[M+H]^+$ 561.2483, found 561.2482.

2.3. Synthetic procedure of (−)-*3*: (−)-*MAD28*

To a stirred solution of (−)-diastereomer **8** (44.0 mg, 0.079 mmol) in THF (1.7 mL) was added aqueous KOH (5 N, 0.15 mL). The reaction mixture was stirred at room temperature for 1.5 h. The onset of an orange-red solution indicated the formation of the free hydroxyl group of **MAD28**. Upon completion, the reaction mixture was diluted with EtOAc and washed with water (3 × 1 mL). The combined EtOAc layers were dried over $MgSO_4$, filtered and concentrated by rotary evaporation. The crude material was purified by flash column chromatography (silica, 13% EtOAc/hexane) to give compound (−)-**3** (26.1 mg, 87%) as a yellow solid.

(−)-**3:** R_f = 0.59 (hexane/EtOAc = 3:1); $[\alpha]_D^{23}$ = –469.1 (*c* = 0.29, $CHCl_3$); ECD (*c* = 78.6 × 10^{-3} mM, MeOH) λ_{max} (deg cm^2 $dmol^{-1}$) 233 (–21565.1), 259 (35547.2), 301 (99562.4), 341 (–131789); ^{1}H NMR (400 MHz, $CDCl_3$) δ 12.08 (s, 1H), 7.48 (d, *J* = 7.0 Hz, 1H), 7.40 (t, *J* = 8.3 Hz, 1H), 6.53 (t, *J* = 8.4 Hz, 2H), 4.41 (t, *J* = 5.9 Hz, 1H), 3.53 (t, *J* = 5.0 Hz, 1H), 2.63 (d, *J* = 9.6 Hz, 2H), 2.45 (d, *J* = 9.6 Hz, 1H), 2.35 (dd, *J* = 13.5, 4.5 Hz, 1H), 1.70 (s, 3H), 1.37 (s, 3H), 1.32–1.30 (m, 1H), 1.30 (s, 3H), 1.01 (s, 3H); ^{13}C NMR (100 MHz, $CDCl_3$) δ 202.8, 181.4, 162.9, 159.6, 138.8, 135.4, 135.0, 133.9, 118.7, 109.4, 107.5, 106.1, 90.0, 84.5, 83.6, 48.8, 47.0, 30.4, 29.23, 29.15, 25.6, 25.0, 16.8; HRMS (ESI) m/e calcd for $[C_{23}H_{23}O_5]^-$ $[M-H]^-$ 379.1551, found 379.1552. The enantiomeric excess of (−)-**3** (t_R 17 min) is 100%.

2.4. Synthetic procedure of (+)-3: (+)-MAD28

To a stirred solution of (+)-diastereomer **9** (22.7 mg, 0.04 mmol) in THF (0.9 mL) was added aqueous KOH (5 N, 0.07 mL). The reaction mixture was stirred at room temperature for 30 min. The onset of an orange-red solution indicated the formation of the free hydroxyl group of **MAD28**. Upon completion, the reaction mixture was diluted with EtOAc and washed with water (3 × 1 mL). The combined EtOAc layers were dried over $MgSO_4$, filtered and concentrated by rotary evaporation. The crude material was purified by flash column chromatography (silica, 13% EtOAc/hexane) to give compound (+)-**3** (12.2 mg, 80%) as a yellow solid.

(+)-3: $R_f = 0.59$ (hexane/EtOAc = 3:1); $[\alpha]_D^{23} = +411.8$ ($c = 0.29$, $CHCl_3$); ECD ($c = 78.6 \times 10^{-3}$ mM, MeOH) λ_{max} (deg cm^2 $dmol^{-1}$) 233 (15968.9), 259 (–27537.9), 301 (–77569.2), 341 (103394); ^1H NMR (400 MHz, $CDCl_3$) δ 12.08 (s, 1H), 7.49 (d, $J = 6.9$ Hz, 1H), 7.40 (t, $J = 8.3$ Hz, 1H), 6.53 (t, $J = 8.8$ Hz, 2H), 4.42 (t, $J = 5.9$ Hz, 1H), 3.53 (t, $J = 5.9$ Hz, 1H), 2.63 (d, $J = 9.5$ Hz, 2H), 2.45 (d, $J = 9.6$ Hz, 1H), 2.35 (dd, $J = 13.6$, 4.5 Hz, 1H), 1.70 (s, 3H), 1.37 (s, 3H), 1.32–1.30 (m, 1H), 1.30 (s, 3H), 1.01 (s, 3H); ^{13}C NMR (125 MHz, $CDCl_3$) δ 202.7, 181.3, 162.8, 159.6, 138.7, 135.3, 134.9, 133.8, 118.6, 109.3, 107.4, 106.1, 90.0, 83.7, 83.5, 48.8, 47.0, 30.3, 29.1, 29.0, 25.5, 24.9, 16.7; HRMS (ESI) m/e calcd for $[C_{23}H_{23}O_5]^-$ $[M-H]^-$ 379.1551, found 379.1550. The enantiomeric excess of (+)-**3** (t_R 18 min) is 94%.

2.5. Cell culture

Cell lines SKBR3, MDA-MB-468, MDA-MB-231, BT474 and MCF-7 were acquired from ATCC and cultured in RPMI containing 10% heat-inactivated fetal bovine serum (HI-FBS) and penicillin/streptomycin. Spheroids$^{MARY\text{-}X}$ were kept in MEM containing 10% HI-FBS and penicillin/streptomycin. HMECs were maintained in mammary epithelial basal media with appropriate supplements (ThermoFisher Scientific, cat# 12755013). All cell lines were maintained in humidified air with 5% CO_2 at 37 °C.

2.6. Viability assays

Cell lines were seeded in opaque 96-well plates at a density of 2000 cells per well. 24 h after seeding, the cells were treated with increasing concentrations of **(+/−)-MAD28**, **(−)-MAD28**, and **(+)-MAD28**. All treatments were performed with freshly prepared 2-fold serial dilutions of the compounds in DMSO at concentrations ranging from 20 to 0.08 μM. Evaluation of cell viability was performed 24 h after treatment using the CellTiter-Glo 3D kit (#G9682) according to the manufacturer's instructions. Luminescence was quantified using a FilterMax F5 Microplate Reader. The luminescence of samples treated with DMSO (control) was set to 100% viability. The viability assays were performed at least 3 times for each cell line with 2 technical replicates for each experiment. Dose-response curves were constructed based on the normalized viability data for each drug treatment using GraphPad Prism version 8.0.2 for Windows. Nonlinear regression curves with variable slopes generated for the different treatments in the same cell line were compared to each other using extra sum-of-squares F test to conclude if the same curve can fit all the data, leading to a global (best fit) curve.

2.7. Immunoblot analysis

Cells seeded in 6-well plates were treated with vehicle only (control; DMSO) and increasing concentrations of racemic **MAD28** and enantiomers. Following 24 h treatment, cells were lysed in RIPA buffer supplemented with HALT protease and phosphatase inhibitors (#78440). Cell lysates were quantified, and 5–10 μg of total protein was prepared for SDS-PAGE. Proteins were transferred to PVDF membrane and blocked with 5% milk for 30 min. Membranes were incubated overnight at 4 °C with primary antibodies, for cleaved-PARP or cleaved-caspase 3 or 7 and actin. Following application of appropriate HRP-conjugated secondary antibodies, membranes were incubated in enhanced chemiluminescence reagents for immunoblot detection.

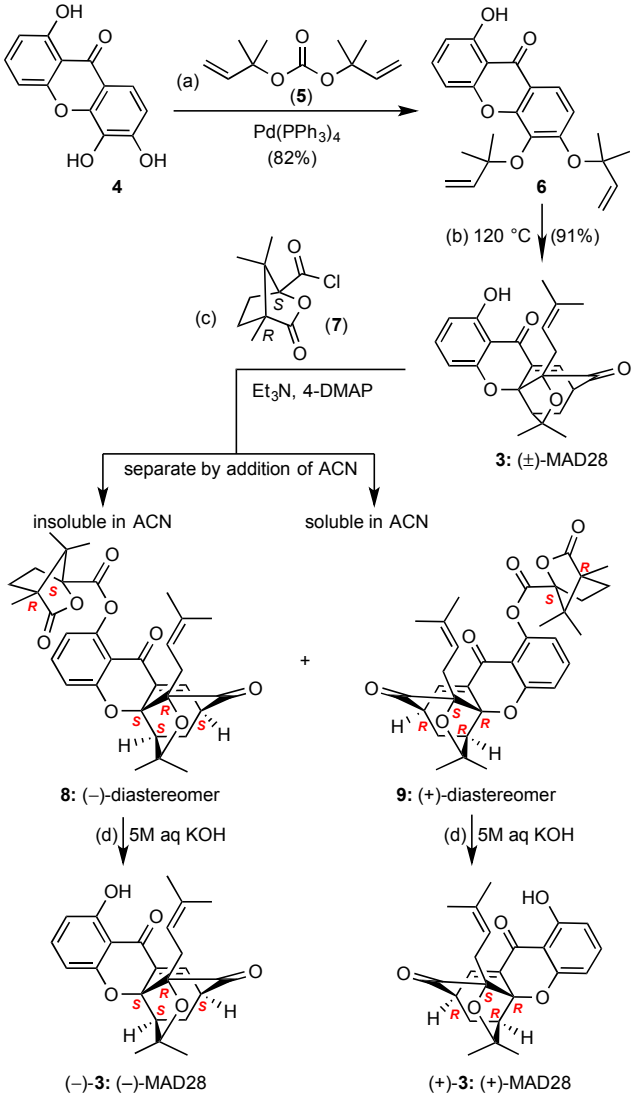

Scheme 1. Reagents and conditions: (a) 6 equiv. bis(2-methylbut-3-en-2-yl) carbonate (**5**), 4 mol% $Pd(PPh_3)_4$, THF, 0 to 5 °C, 4.5 h, 82%; (b) DMF, 6 h, 120 °C, 91%; (c) 1.9 equiv. (1*S*, 4*R*)-(−)-camphanic chloride, 4 equiv. Et_3N, 1 equiv. 4-DMAP, CH_2Cl_2, 4 h, 25 °C, 48% for **8** and 32% for **9**; (d) 5 M aq KOH, THF, 25 °C, 1.5 h, 87% for (−)-**3** and 0.5 h, 80% for (+)-**3**.

3. Results and discussion

3.1. Synthesis and chiral resolution of (+/−)-MAD28

The synthesis of **MAD28** (**3**) was performed by the two-step sequence that involves Pd(0)-catalyzed reverse prenylation of **4** with carbonate **5** and heat-induced Claisen/Diels–Alder reaction of **6** (Scheme 1) [37]. The chiral HPLC chromatogram of **3** shows well-resolved peaks at t_R of 17 and 18 min in an approximate ratio of 1:1 (50.3% : 49.7%) (Fig. 2A), showing that indeed, **3** is a racemic mixture. This mixture was resolved using (1*S*, 4*R*)-(−)-camphanic chloride (**7**) as a chiral agent [56,57] to form a mixture of diastereomeric esters **8** and **9**. Addition of acetonitrile to the mixture of these isomers resulted in precipitation of compound **8** that could be filtered from the solution. Diastereoisomer **9** remained in the solution and was subsequently

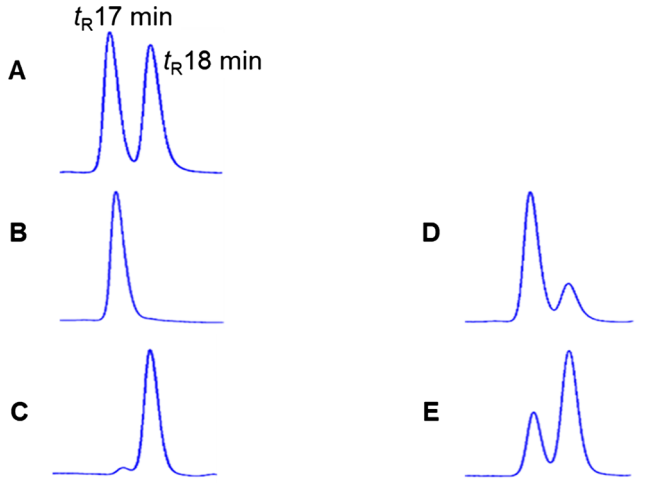

Fig. 2. Chiral HPLC chromatograms using a Lux® 5 μm Amylose-2 (250 × 4.6 mm) column with detection at 250 nm, 50% ACN/H_2O as eluent and a flow rate of 1.2 mL/min. (A) **3: MAD28**; (B) (−)-**3** (t_R17 min); (C) (+)-**3** (t_R18 min); (D) co-injection of **3** and (−)-**3**; (E) co-injection of **3** and (+)-**3**.

purified by silica gel column chromatography. Basic hydrolysis of **8** and **9**, led to isolation of (−)-**3** ($[\alpha]_D^{23}$ = –469.1, *c* = 0.29, $CHCl_3$) and (+)-**3** ($[\alpha]_D^{23}$ = +411.8, *c* = 0.29, $CHCl_3$), respectively.

The enantiomeric purity determination of (−)-**3** and (+)-**3** was performed via chiral HPLC analysis (Fig. 2). The chiral HPLC chromatogram of (−)-**3** reveals a single enantiomer with an enantiomeric excess of 100% (Fig. 2B). On the other hand, the chiral HPLC chromatogram of (+)-**3** shows two peaks in a ratio of 3:97, indicating that the enantiomeric excess of (+)-**3** is 94% (Fig. 2C). In addition, the elution order of the enantiomers (−)-**3** and (+)-**3** was confirmed by co-injection of **3** and (−)-**3** as well as co-injection of **3** and (+)-**3** (Fig. 2D and 2E, respectively).

To establish the absolute configuration, single crystals of **8** and (−)-**3** were subjected to X-ray structure analysis using Cu Kα radiation (Fig. 3). Based on the X-ray data analysis, the absolute configuration of **8** and (−)-**3** was assigned as 11*S*, 13*R*, 14*S* and 22*S* [58]. The results are consistent with previous reports on the absolute configuration of caged motif presented in (−)-morellic acid and (−)-gambogic acid [59,60].

The electronic circular dichroism (ECD) spectrum of (−)-**3** (Fig. 4, blue line) shows a positive Cotton effect near 259 and 301 nm and a negative Cotton effect near 233 and 341 nm, whereas the ECD spectrum of (+)-**3** (Fig. 4, red line) displays Cotton effects of the opposite signs. These results indicate that the absolute configuration of (+)-**3** is 11*R*, 13*S*, 14*R* and 22*R*.

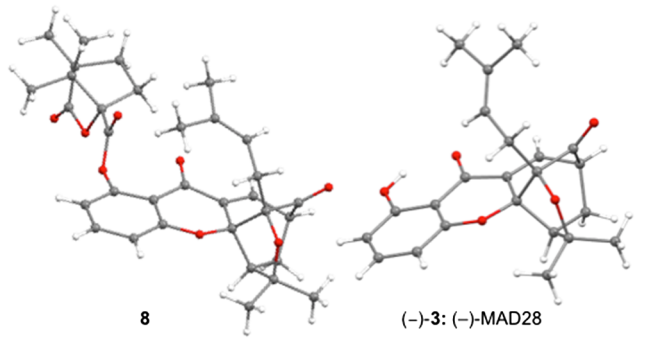

Fig. 3. X-ray structures of ester **8** and (−)-**MAD28**.

3.2. Enantiomer evaluation across a broad spectrum of breast cancer cell line subtypes

Histopathological analysis and DNA microarray profiling have demonstrated that breast cancer is highly heterogeneous [61–63]. Based on immunostaining and protein expression there are at least five distinct subtypes, commonly referred to as: HER2, luminal A, luminal B, claudin-low and basal [64,65]. With this in mind, we evaluated the bioactivity of **MAD28** and its enantiomers across a broad panel of breast cancer cell lines. Cells were seeded in a multi-well plate at the optimum cell density/number and treated with vehicle only (DMSO) and increasing drug concentrations (0.08–20.0 μM) of the racemic mixture and each of the enantiomers. The treated plate was incubated for 24 h under standard tissue culture conditions. Experiments were conducted in triplicates. Following treatment, viability for each cell line was assessed using a CellTiter-Glo 3D ATP quantitation kit. The IC_{50} was determined from dose-response curves constructed for each breast cancer subtype (Fig. 5, Fig. S1 and Table 1).

The IC_{50} calculated via ATP quantitation for spheroids$^{MARY\text{-}X}$ (0.7 +/− 0.1 μM) is comparable to the IC_{50} values previously calculated for the racemic **MAD28** (0.66 +/− 0.22 μM) using spheroid dissolution indices (i.e., response measured as a deviation from a well-circumscribed spheroid edge) [42,43]. Dissolution of the formerly intact spheroids$^{MARY\text{-}X}$ following treatment with **(+/−)-MAD28** and enantiomers is shown in Fig. 6. Dissolution is an alternate means for viability assessment and IC_{50} evaluation, where dissolute spheroids or single cell suspension is indicative of cell death. Thus, the response of IBC spheroids$^{MARY\text{-}X}$ to **MAD28** is now validated by two different cell viability assays (ATP quantitation vs. dissolution indices).

Table 1 summarizes the IC_{50} values for **(+/−)-MAD28** and its enantiomers across six breast cancer cell lines representing five molecularly distinct subtypes and MARY-X, a 3D triple negative inflammatory breast cancer model. The best fit IC_{50} represents a global curve that adequately fits all the data sets collected from the racemic **MAD28** and its enantiomers per treated cell line. The IC_{50} data indicate that racemic **MAD28** is equipotent with its purified enantiomers in each of the molecularly-defined breast cancer subtypes (Table 1 and Fig. S1). It is interesting to observe that cell lines which overexpress human epidermal growth factor receptor-2 (HER2), such as SKBR3, as well as BT474 which overexpresses HER2, estrogen (ER) and sometimes progesterone (PR) receptors, are less sensitive to **MAD28** than cells of basal-like subtype with a triple negative receptor status, such as the MDA-MB-468 cell line (Fig. 5). In fact, there is approximately 2-fold higher efficacy (1.6 μM IC_{50} vs. 3.5 μM IC_{50}) between the basal vs. the HER2 enriched and luminal B subtypes, respectively (Fig. 5A-C). Moreover, sub-micromolar response was measured in the triple negative 3D inflammatory breast cancer model, spheroids$^{MARY\text{-}X}$ with an IC_{50} of 0.7 μM (Table 1 and Fig. 5D). In addition, the therapeutic index (*in vitro;* HMEC IC_{50}/BC IC_{50}) was calculated for each breast cancer cell line (Table 1) using the normal human mammary epithelial cells (ESI Fig. S2).

The SKBR3 cell line represents a breast cancer subtype that does not overexpress estrogen and progesterone receptors (ER−, PR−). This subtype is however, defined by the presence of human epidermal growth factor receptor-2 (HER2+) which is an established therapeutic target [66]. As such it can be treated with trastuzumab (Herceptin) and related combination therapies. MCF7 cells are representative of the luminal A subtype in which HER2 is not expressed. Nonetheless, these cancer cells overexpress ERs and sometimes PRs thus allowing for anti-estrogen based therapeutic strategies [67]. In general, these cells have low levels of Ki-67, a marker of tumor cell growth and division [68]. Based on this, they are considered low grade and grow slowly. BT474 cells are representative of the luminal B subtype and overexpress ERs (and/or PRs) [69,70]. These cells are HER2 positive with high levels of Ki-67 [65,71]. As such, they grow faster than luminal A cancers and have worse prognosis. The MDA-MB-231 cell line is a representative of

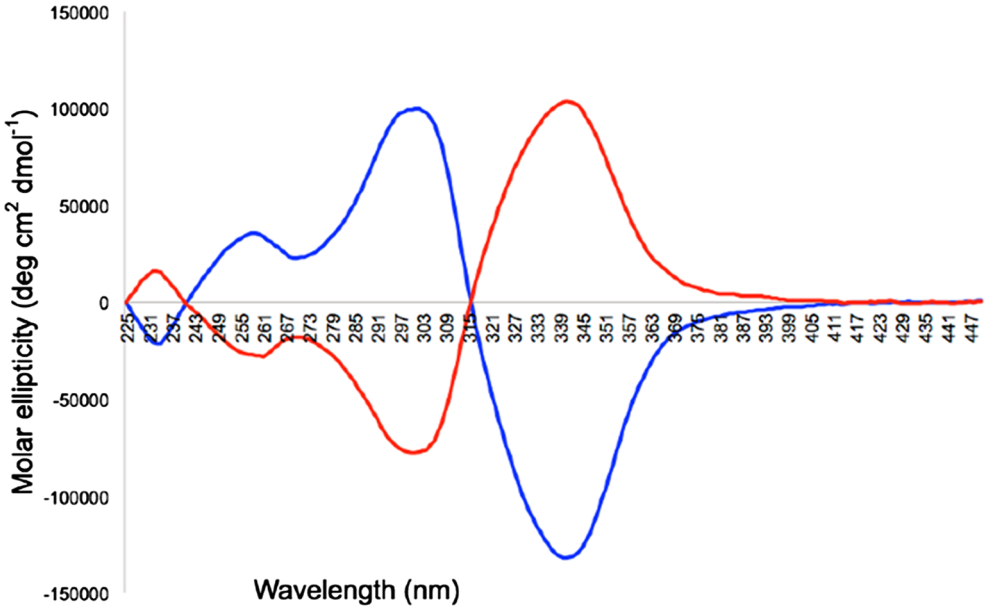

Fig. 4. ECD spectra of compounds (−)-**3** (blue line) and (+)-**3** (red line) in MeOH (78.6×10^{-3} mM).

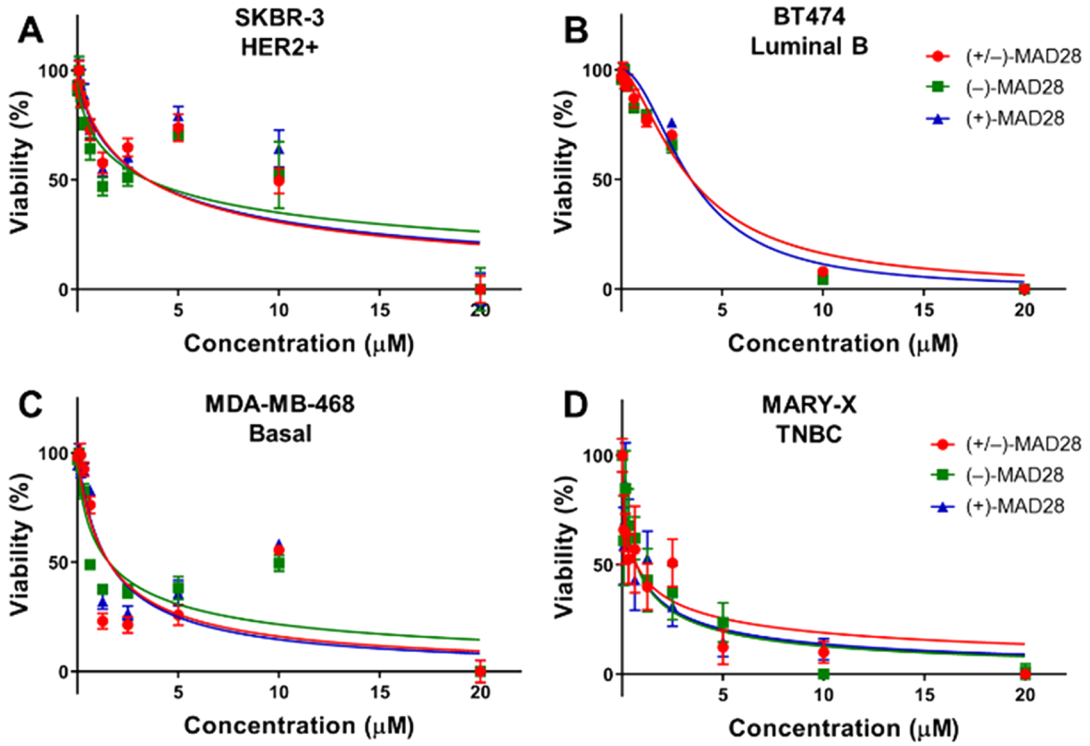

Fig. 5. Dose-response curves of racemic MAD28 and enantiomers against various breast cancer molecular subtypes: (A) SKBR3 cell line (HER2+); (B) BT474 cell line (Luminal B; ER + PR+/−HER2+); (C) MDA-MB-468 cell line (basal; triple negative); and (D) Spheroids$^{MARY\text{-}X}$ (3-D; triple negative).

triple negative receptor status since it does not express ER, PR and HER2 on its cell surface [72]. These cells downregulate claudin-3, -4 and -7, proteins involved in cell invasion and metastasis [65,73] and also have low expression of Ki67 [71]. Similarly, the MDA-MB-468 cell line represents the basal-like breast cancer subtype that is defined by negative immunohistochemical staining for ER, PR and HER2 [74–76]. These cells show high levels of Ki67 and strong expression of basal markers such as cytokeratins 5,6 and 17 [77,78]. This type of cancer is more common in women with BRCA1 gene mutations, has poor clinical outcomes and shows disproportionately higher prevalence in women of African descent. The spheroids$^{MARY\text{-}X}$ are a representative *in vitro* model of inflammatory breast cancer (IBC), the most lethal and aggressive form of breast disease that is stage 4 upon diagnosis. IBC does not have any known molecular diagnostic criteria and hence, there are no known IBC-specific targeted therapies [48,49,79]. Interestingly, gene expression studies of IBC tumors has revealed an enrichment in basal-like subtype providing a reasonable explanation for the similar sensitivity of spheroids$^{MARY\text{-}X}$ and MDA-MB-468 to **MAD28.**

The effect of **(+/−)-MAD28** and its enantiomers on cell death was assessed by immunoblot analysis of the apoptotic pathway markers cleaved-poly ADP-ribose polymerase (c-PARP) and cleaved-caspase 3 or 7 [80,81]. A dose-dependent increase in appearance of both c-PARP

Table 1
Calculated IC_{50} values and *in vitro* therapeutic indices (TI) for representative breast cancer cell lines.

Cell line	Classification	Receptor status	IC_{50} (μM)				TI
			(+/−)-MAD28	(−)-MAD28	(+)-MAD28	Best fit IC_{50}	
SKBR3	HER2	ER−, PR−, HER2+	**3.7** +/−0.7	**3.0** +/−0.8	**3.7** +/−0.8	**3.5** +/−0.4	**1.1**
BT474	Luminal B	ER+, PR+/−, HER2+	**3.5** +/−0.3	**3.1** +/−0.2	**3.8** +/−0.2	**3.5** +/−0.1	**1.1**
MDA-MB-231	Claudin-low	ER−, PR−, HER2−	**3.4** +/−0.3	**3.0** +/−0.2	**3.3** +/−0.3	**3.2** +/−0.2	**1.3**
MCF-7	Luminal A	ER+, PR+/−, HER2−	**2.2** +/−0.2	**2.1** +/−0.2	**2.7** +/−0.3	**2.3** +/−0.1	**1.7**
MDA-MB-468	Basal	ER−, PR−, HER2−	**1.4** +/−0.2	**1.4** +/−0.2	**1.9** +/−0.3	**1.6** +/−0.2	**2.5**
MARY-X	3D	ER−, PR−, HER2−	**0.6** +/−0.2	**0.9** +/−0.3	**0.7** +/−0.2	**0.7** +/−0.1	**5.7**

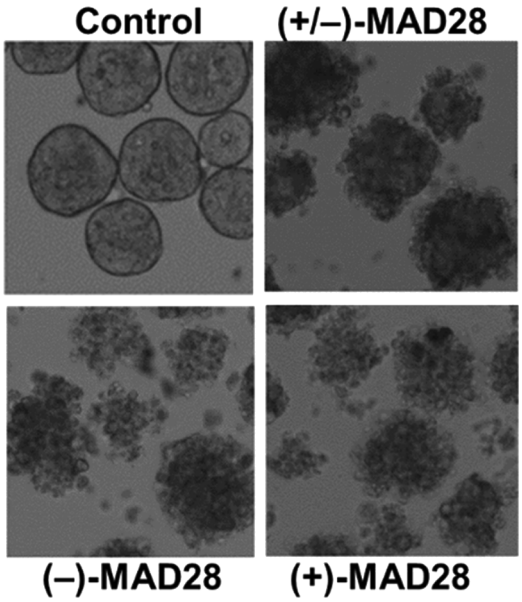

Fig. 6. Dissolution of spheroids$^{MARY\text{-}X}$ following treatment with racemic MAD28 and enantiomers: Control (vehicle only; DMSO) following 24 h period shows well-circumscribed spheroid edges. Racemic **(+/−)-MAD28**, and both enantiomers, **(−)-MAD28** and **(+)-MAD28** treated spheroids (2.25 μM) display equipotency resulting in total dissolution of formerly intact spheroids indicative of cell death.

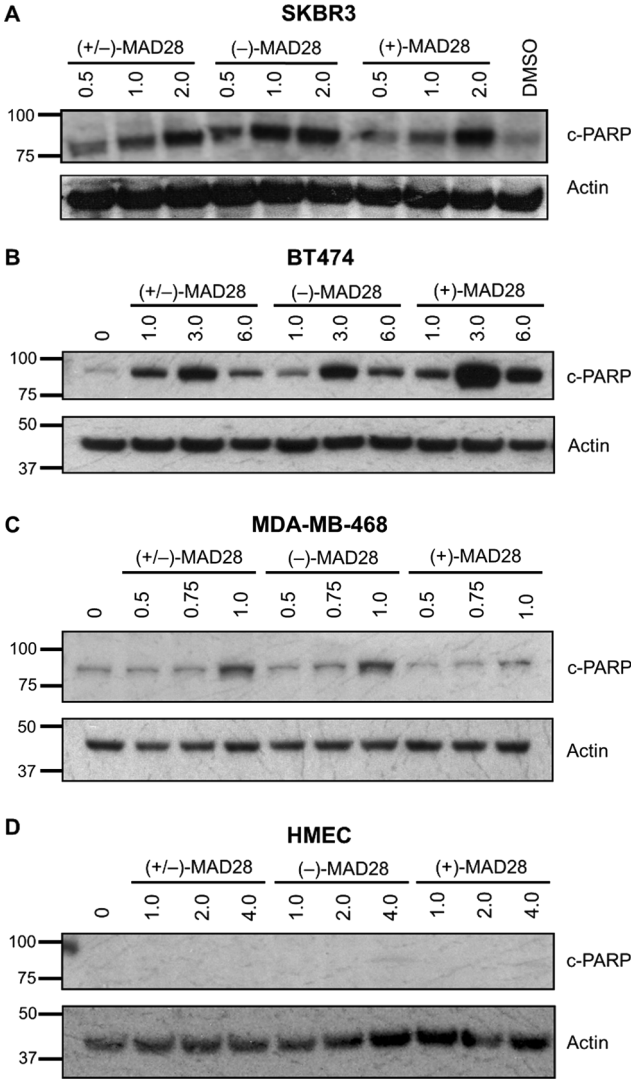

Fig. 7. Apoptosis evaluation of BC cell lines as compared to a normal cell line (HMEC) following treatment with racemic MAD28 and enantiomers: **(A)** SKBR3 cell line (HER+), **(B)** BT474 cell line (Luminal B; ER+PR+/−HER2+) and **(C)** MDA-MB 468 cell line (basal; triple negative) display dose-dependent apoptotic response with increase in c-PARP. **(D)** Human mammary epithelial cells (HMEC) do not display induction of apoptosis.

(Fig. 7A-C) and cleaved-caspase 3 or 7 (Fig. S3) was seen across all molecular breast cancer subtypes irrespective of treatment with racemic **MAD28** or its enantiomers. Control experiments were also performed using human mammary epithelial cells (HMEC), a normal primary cell line. Treatment of these cells with up to 4.0 μM **MAD28** showed no production of c-PARP and thus, no induction of apoptosis (Fig. 7D). In turn, this supports the notion that these compounds are selectively cytotoxic against aggressive and metastatic breast cancer cell lines [37].

4. Conclusions

We report here the chiral resolution of **(+/−)-MAD28** to its enantiomers using camphanic chloride as the resolving agent. The resulting diastereomers can be separated via selective precipitation in acetonitrile giving rise, after hydrolysis, to the corresponding enantiomers. This approach may also be applicable to other caged xanthones containing free phenol groups and, at the absence of any enantioselective synthesis, it provides a straightforward way to access enantiomerically pure compounds. We also compared the bioactivity of these enantiomers in a broad panel of breast cancer cell lines that represent the various breast cancer subtypes. We found that both enantiomers and the racemic mixture of **MAD28** are equipotent across each cell line. Importantly, the IC_{50} values decrease by more than 2-fold in breast cancer cell lines that are characterized by a triple negative receptor status and high proliferative status (Ki67), both indicative of an aggressive phenotype. In fact, the lowest IC_{50} values were measured in spheroids$^{MARY\text{-}X}$, an *in vitro* model of inflammatory breast cancer that is characterized by a triple negative receptor status with a chemoresistant and highly metastatic phenotype. The results indicate that **MAD28** exerts selective cytotoxicity in aggressive, chemorefractory breast cancer that lacks actionable targets. In turn, this provides

additional support in identifying **MAD28** and related caged xanthones as promising drug leads for chemoresistant and metastatic cancers.

Declaration of Competing Interest

There are no conflicts to declare.

Acknowledgments

We thank the financial support of the California Breast Cancer Research Program (IDEA Award No: 22IB-0024). This work was also supported by the Ellington Beavers Award from Arcadia University. We also thank Professor T. F. Molinski (UCSD) for access to his chiral HPLC columns and Teresa Abendroth for editorial assistance.

Appendix A. Supplementary material

The Supporting Information to this article can be found online. It contains: **Fig. S1** Dose-response curves for all breast cancer cell lines; **Fig. S2** Dose-response curve for the normal human mammary epithelial cells (HMEC); **Fig. S3** Analysis of apoptosis via western blot. It also contains: (a) chemical procedures, characterization data and ^{1}H and ^{13}C NMR spectra for compounds **6** and **(+/−)-MAD28**; (b) ^{1}H and ^{13}C NMR spectra of **8 9**, **(−)-MAD28** and **(+)-MAD28**; and (c) tables with X-ray data for **8** and **(−)-3**. Supplementary data to this article can be found online at https://doi.org/10.1016/j.bioorg.2019.103303.

References

[1] N. Anantachoke, P. Tuchinda, C. Kuhakarn, M. Pohmakotr, V. Reutrakul, Prenylated caged xanthones: chemistry and biology, Pharm. Biol. 50 (1) (2012) 78.
[2] O. Chantarasriwong, A. Batova, W. Chavasiri, E. Theodorakis, Chemistry and biology of the caged garcinia xanthones, Chem. – A Eur. J. 16 (2010) 9944.
[3] B. Jia, S. Li, X. Hu, G. Zhu, W. Chen, Recent research on bioactive xanthones from natural medicine: Garcinia hanburyi, AAPS PharmSciTech 16 (4) (2015) 742.
[4] S. Alam, F. Khan, Virtual screening, docking, ADMET and system pharmacology studies on garcinia caged xanthone derivatives for anticancer activity, Sci. Rep. 8 (1) (2018) 5524.
[5] J. Araújo, C. Fernandes, M. Pinto, M.E. Tiritan, Chiral derivatives of xanthones with antimicrobial activity, Molecules 24 (2) (2019) 314.
[6] C. Fernandes, M.L. Carraro, J. Ribeiro, J. Araújo, M.E. Tiritan, M.M.M. Pinto, Synthetic chiral derivatives of xanthones: biological activities and enantioselectivity studies, Molecules 24 (4) (2019) 791.
[7] V. Reutrakul, N. Anantachoke, M. Pohmakotr, T. Jaipetch, S. Sophasan, C. Yoosook, J. Kasisit, C. Napaswat, T. Santisuk, P. Tuchinda, Cytotoxic and anti-HIV-1 caged xanthones from the resin and fruits of Garcinia hanburyi, Planta Med. 73 (1) (2007) 33.
[8] V. Rukachaisirikul, P. Phainuphong, Y. Sukpondma, S. Phongpaichit, W.C. Taylor, Antibacterial caged-tetraprenylated xanthones from the stem bark of Garcinia scortechinii, Planta Med. 71 (2) (2005) 165.
[9] Y. Sukpondma, V. Rukachaisirikul, S. Phongpaichit, Antibacterial caged-tetraprenylated xanthones from the fruits of Garcinia hanburyi, Chem. Pharm. Bull. 53 (7) (2005) 850.
[10] S.-J. Tao, S.-H. Guan, W. Wang, Z.-Q. Lu, G.-T. Chen, N. Sha, Q.-X. Yue, X. Liu, D.-A. Guo, Cytotoxic polyprenylated xanthones from the resin of Garcinia hanburyi, J. Nat. Prod. 72 (1) (2009) 117.
[11] H. Ke, J.M. Morrisey, S. Qu, O. Chantarasriwong, M.W. Mather, E.A. Theodorakis, A.B. Vaidya, Caged Garcinia xanthones, a novel chemical scaffold with potent antimalarial activity, Antimicrob. Agents Chemother. 61 (1) (2017) e01220.
[12] Q. Guo, Q. Qi, Q. You, H. Gu, L. Zhao, Z. Wu, Toxicological studies of gambogic acid and its potential targets in experimental animals, Basic Clin. Pharmacol. Toxicol. 99 (2) (2006) 178.
[13] L. Zhao, C. Zhen, Z. Wu, R. Hu, C. Zhou, Q. Guo, General pharmacological properties, developmental toxicity, and analgesic activity of gambogic acid, a novel natural anticancer agent, Drug Chem. Toxicol. 33 (1) (2010) 88.
[14] Q. Qi, Q. You, H. Gu, L. Zhao, W. Liu, N. Lu, Q. Guo, Studies on the toxicity of gambogic acid in rats, J. Ethnopharmacol. 117 (3) (2008) 433.
[15] K. Hao, X.-Q. Liu, G.-J. Wang, X.-P. Zhao, Pharmacokinetics, tissue distribution and excretion of gambogic acid in rats, Eur. J. Drug Metab. Pharmacokinet. 32 (2) (2007) 63.
[16] K. Banik, C. Harsha, D. Bordoloi, B. Lalduhsaki Sailo, G. Sethi, H.C. Leong, F. Arfuso, S. Mishra, L. Wang, A.P. Kumar, et al., Therapeutic potential of gambogic acid, a caged xanthone, to target cancer, Cancer Lett. 416 (2018) 75.
[17] L. Liang, Z. Zhang, X. Qin, Y. Gao, P. Zhao, J. Liu, W. Zeng, Gambogic acid inhibits melanoma through regulation of miR-199a-3p/ZEB1 signalling, Basic Clin. Pharmacol. Toxicol. 123 (6) (2018) 692.
[18] Y. Chi, X.K. Zhan, H. Yu, G.R. Xie, Z.Z. Wang, W. Xiao, Y.G. Wang, F.X. Xiong, J.F. Hu, L. Yang, et al., An open-labeled, randomized, multicenter phase IIa study of gambogic acid injection for advanced malignant tumors, Chin. Med. J. 126 (2013) 1642.
[19] L.H. Wang, Y. Li, S.N. Yang, F.Y. Wang, Y. Hou, W. Cui, K. Chen, Q. Cao, S. Wang, T.Y. Zhang, et al., Gambogic acid synergistically potentiates cisplatin-induced apoptosis in non-small-cell lung cancer through suppressing NF-[kappa]B and MAPK/HO-1 signalling, Br. J. Cancer 110 (2) (2014) 341.
[20] H.B. Huang, D. Chen, S.J. Li, X.F. Li, N.N. Liu, X.Y. Lu, S.T. Liu, K. Zhao, C.G. Zhao, H.P. Guo, et al., Gambogic acid enhances proteasome inhibitor-induced anticancer activity, Cancer Lett. 301 (2) (2011) 221.
[21] X.F. Li, S.T. Liu, H.B. Huang, N.N. Liu, C. Zhao, S.Y. Liao, C.S. Yang, Y.R. Liu, C.G. Zhao, S.J. Li, et al., Gambogic acid is a tissue-specific proteasome inhibitor in vitro and in vivo, Cell Rep 3 (1) (2013) 211.
[22] Y.X. Qin, L.H. Meng, C.X. Hu, W.H. Duan, Z.L. Zuo, L.P. Lin, X.W. Zhang, J. Ding, Gambogic acid inhibits the catalytic activity of human topoisomerase II alpha by binding to its ATPase domain, Mol. Cancer Ther. 6 (9) (2007) 2429.
[23] D.Y. Zhai, C.F. Jin, C.W. Shiau, S. Kitada, A.C. Satterthwait, J.C. Reed, Gambogic acid is an antagonist of antiapoptotic Bcl-2 family proteins, Mol. Cancer Ther. 7 (6) (2008) 1639.
[24] L. Zhao, Q.-L. Guo, Q.-D. You, Z.-Q. Wu, H.-Y. Gu, Gambogic acid induces apoptosis and regulates expressions of bax and Bcl-2 protein in human gastric carcinoma MGC-803 cells, Biol. Pharm. Bull. 27 (7) (2004) 998.
[25] J. Davenport, J.R. Manjarrez, L. Peterson, B. Krumm, B.S.J. Blagg, R.L. Matts, Gambogic acid, a natural product inhibitor of Hsp90, J. Nat. Prod. 74 (5) (2011) 1085.
[26] K.M. Elbel, G. Guizzunti, M.A. Theodoraki, J. Xu, A. Batova, M. Dakanali, E.A. Theodorakis, A-ring oxygenation modulates the chemistry and bioactivity of caged Garcinia xanthones, Org. Biomol. Chem. 11 (20) (2013) 3341.
[27] K.H. Yim, T.L. Prince, S.W. Qu, F. Bai, P.A. Jennings, J.N. Onuchic, E.A. Theodorakis, L. Neckers, Gambogic acid identifies an isoform-specific druggable pocket in the middle domain of Hsp90 beta, P. Natl. Acad. Sci. USA 113 (33) (2016) E4801.
[28] Q. Yue, F. Stahl, O. Plettenburg, A. Kirschning, A. Warnecke, C. Zeilinger, The noncompetitive effect of gambogic acid displaces fluorescence-labeled ATP but requires ATP for binding to Hsp90/HtpG, Biochemistry 57 (18) (2018) 2601.
[29] G. Guizzunti, A. Batova, O. Chantarasriwong, M. Dakanali, E.A. Theodorakis, Subcellular localization and activity of gambogic acid, ChemBioChem 13 (8) (2012) 1191.
[30] L.L. Liang, Z.X. Zhang, Gambogic acid inhibits malignant melanoma cell proliferation through mitochondrial p66(shc)/ROS-p53/Bax-mediated apoptosis, Cell. Physiol. Biochem. 38 (4) (2016) 1618.
[31] F. Nie, X. Zhang, Q. Qi, L. Yang, Y. Yang, W. Liu, N. Lu, Z. Wu, Q. You, Q. Guo, Reactive oxygen species accumulation contributes to gambogic acid-induced apoptosis in human hepatoma SMMC-7721 cells, Toxicology 260 (1–3) (2009) 60.
[32] J.Y. Xu, M. Zhou, J. Ouyang, J. Wang, Q.G. Zhang, Y. Xu, Y.Y. Xu, Q. Zhang, X.H. Xu, H. Zeng, Gambogic acid induces mitochondria-dependent apoptosis by modulation of Bcl-2 and Bax in mantle cell lymphoma JeKo-1 cells, Chinese J. Cancer Res. 25 (2) (2013) 183.
[33] J. Yang, C.L. Li, L. Ding, Q.L. Guo, Q.D. You, S.H. Jin, Gambogic acid deactivates cytosolic and mitochondrial thioredoxins by covalent binding to the functional domain, J. Nat. Prod. 75 (6) (2012) 1108.
[34] M.J. Seo, D.M. Lee, I.Y. Kim, D. Lee, M.K. Choi, J.Y. Lee, S.S. Park, S.Y. Jeong, E.K. Choi, K.S. Choi, Gambogic acid triggers vacuolization-associated cell death in cancer cells via disruption of thiol proteostasis, Cell Death Dis. 10 (3) (2019) 187.
[35] O. Chantarasriwong, W.C. Cho, A. Batova, W. Chavasiri, C. Moore, A.L. Rheingold, E.A. Theodorakis, Evaluation of the pharmacophoric motif of the caged Garcinia xanthones, Org. Biomol. Chem. 7 (23) (2009) 4886.
[36] O. Chantarasriwong, B.D. Althufairi, N.J. Checchia, E.A. Theodorakis, Chapter 4 - Caged Garcinia Xanthones: Synthetic Studies and Pharmacophore Evaluation, Studies in Natural Products Chemistry, 58 Elsevier, 2018, pp. 93–131.
[37] F. Bai, F. Morcos, J.N. Onuchic, Y.-S. Sohn, M. Darash-Yahana, S. Tamir, C.O. Rezende, C.H. Lipper, M.L. Paddock, E.A. Theodorakis, et al., The Fe-S cluster-containing NEET proteins mitoNEET and NAF-1 as chemotherapeutic targets in breast cancer, Proc. Natl. Acad. Sci. U.S.A. 112 (12) (2015) 3698.
[38] H. Sun, F. Chen, X. Wang, Z. Liu, Q. Yang, X. Zhang, J. Zhu, L. Qiang, Q. Guo, Q. You, Studies on gambogic acid (IV): Exploring structure-activity relationship with IκB kinase-beta (IKKβ), Eur. J. Med. Chem. 51 (2012) 110.
[39] E.J. Tisdale, C. Chowdhury, B.G. Vong, H. Li, E.A. Theodorakis, Regioselective synthesis of the bridged tricyclic core of Garcinia natural products via intramolecular aryl acrylate cycloadditions, Org. Lett. 4 (6) (2002) 909.
[40] X. Wang, N. Lu, Q. Yang, D. Gong, C. Lin, S. Zhang, M. Xi, Y. Gao, L. Wei, Q. Guo, et al., Studies on chemical modification and biology of a natural product, gambogic acid (III): Determination of the essential pharmacophore for biological activity, Eur. J. Med. Chem. 46 (4) (2011) 1280.
[41] X. Li, Y. Wu, Y. Wang, Q. You, X. Zhang, 'Click Chemistry' synthesis of novel natural product-like caged xanthones bearing a 1,2,3-triazole moiety with improved druglike properties as orally active antitumor agents, Molecules 22 (11) (2017) 1834.
[42] O. Chantarasriwong, A.T. Milcarek, T.H. Morales, A.L. Settle, C.O. Rezende Jr., B.D. Althufairi, M.A. Theodoraki, M.L. Alpaugh, E.A. Theodorakis, Synthesis, structure-activity relationship and in vitro pharmacodynamics of A-ring modified caged xanthones in a preclinical model of inflammatory breast cancer, Eur. J. Med. Chem. 168 (2019) 405.
[43] M.A. Theodoraki, C.O. Rezende Jr., O. Chantarasriwong, A.D. Corben, E.A. Theodorakis, M.L. Alpaugh, Spontaneously-forming spheroids as an in vitro cancer cell model for anticancer drug screening, Oncotarget. 6 (25) (2015) 21255.

[44] B. Lim, W.A. Woodward, X. Wang, J.M. Reuben, N.T. Ueno, Inflammatory breast cancer biology: the tumour microenvironment is key, Nat. Rev. Cancer 18 (8) (2018) 485.
[45] D.J. van Uden, H.W. van Laarhoven, A.H. Westenberg, J.H. de Wilt, C.F. Blanken-Peeters, Inflammatory breast cancer: an overview, Crit. Rev. Oncol. Hematol. 93 (2) (2015) 116.
[46] W.A. Woodward, Inflammatory breast cancer: unique biological and therapeutic considerations, Lancet Oncol. 16 (15) (2015) e568.
[47] H. Yamauchi, W.A. Woodward, V. Valero, R.H. Alvarez, A. Lucci, T.A. Buchholz, T. Iwamoto, S. Krishnamurthy, W. Yang, J.M. Reuben, et al., Inflammatory breast cancer: what we know and what we need to learn, Oncologist 17 (7) (2012) 891.
[48] R. Costa, C.A. Santa-Maria, G. Rossi, B.A. Carneiro, Y.K. Chae, W.J. Gradishar, F.J. Giles, M. Cristofanilli, Developmental therapeutics for inflammatory breast cancer: Biology and translational directions, Oncotarget 8 (7) (2017) 12417.
[49] D. Makower, J.A. Sparano, How do I treat inflammatory breast cancer? Curr. Treat. Options Oncol. 14 (1) (2013) 66.
[50] N. Boonnak, S. Chantrapromma, H.-K. Fun, S. Yuenyongsawad, B.O. Patrick, W. Maneerat, D.E. Williams, R.J. Andersen, Three types of cytotoxic natural caged-scaffolds: pure enantiomers or partial racemates, J. Nat. Prod. 77 (7) (2014) 1562.
[51] S.L. Niu, D.H. Li, X.Y. Li, Y.T. Wang, S.G. Li, J. Bai, Y.H. Pei, Y.K. Jing, Z.L. Li, H.M. Hua, Bioassay- and chemistry-guided isolation of scalemic caged prenylxanthones from the leaves of garcinia bracteata, J. Nat. Prod. 81 (4) (2018) 749.
[52] T. Sriyatep, R.J. Andersen, B.O. Patrick, S.G. Pyne, C. Muanprasat, S. Seemakhan, S. Borwornpinyo, S. Laphookhieo, Scalemic caged xanthones isolated from the stem bark extract of garcinia propinqua, J. Nat. Prod. 80 (5) (2017) 1658.
[53] T. Sriyatep, C. Tantapakul, R.J. Andersen, B.O. Patrick, S.G. Pyne, C. Muanprasat, S. Seemakhan, S. Borwornpinyo, S. Laphookhieo, Resolution and identification of scalemic caged xanthones from the leaf extract of Garcinia propinqua having potent cytotoxicities against colon cancer cells, Fitoterapia 124 (2018) 34.
[54] O. Thoison, J. Fahy, V. Dumontet, A. Chiaroni, C. Riche, M.V. Tri, T. Sevenet, Cytotoxic prenylxanthones from garcinia bracteata, J. Nat. Prod. 63 (4) (2000) 441.
[55] B.J. Zhang, W.W. Fu, R. Wu, J.L. Yang, C.Y. Yao, B.X. Yan, H.S. Tan, C.W. Zheng, Z.J. Song, H.X. Xu, Bioactive scalemic caged xanthones from the leaves of Garcinia bracteata, Bioorg. Chem. 82 (2019) 274.
[56] K.M. Cheung, S.J. Coles, M.B. Hursthouse, N.I. Johnson, P.M. Shoolingin-Jordan, The determination of the absolute configurations of diastereomers of (S)camphanoyl 3-hydroxy-5-oxohexanoic acid derivatives by X-ray crystallography, Angew. Chem. Int. Ed. 41 (7) (2002) 1198.
[57] H. Licea-Perez, S. Wang, C. Rodgers, C.L. Bowen, K. Fang, M. Szapacs, C.A. Evans, Camphanic acid chloride: a powerful derivatization reagent for stereoisomeric separation and its DMPK applications, Bioanalysis 7 (23) (2015) 3005.
[58] CCDC 1815139 and CCDC 1815363 contain the supplementary crystallographic data for compounds (–)-3 and 8. These data can be obtained free of charge from the Cambridge Crystallographic Data Centre via http://www.ccdc.cam.ac.uk/products/csd/request/.
[59] Y. Ren, D.D. Lantvit, E.J. Carcache de Blanco, L.B.S. Kardono, S. Riswan, H. Chai, C.E. Cottrell, N.R. Farnsworth, S.M. Swanson, Y. Ding, et al., Proteasome-inhibitory and cytotoxic constituents of Garcinia lateriflora: absolute configuration of caged xanthones, Tetrahedron 66 (29) (2010) 5311.
[60] Y.L. Ren, C.H. Yuan, H.B. Chai, Y.Q. Ding, X.C. Li, D. Ferreira, A.D. Kinghorn, Absolute configuration of (-)-gambogic acid, an antitumor agent, J. Nat. Prod. 74 (3) (2011) 460.
[61] N. Cancer Genome Atlas, Comprehensive molecular portraits of human breast tumours, Nature 490 (7418) (2012) 61.
[62] C. Joseph, A. Papadaki, M. Althobiti, M. Alsaleem, M.A. Aleskandarany, E.A. Rakha, Breast cancer intratumour heterogeneity: current status and clinical implications, Histopathology 73 (5) (2018) 717.
[63] G. Turashvili, E. Brogi, Tumor heterogeneity in breast cancer, Front. Med. (Lausanne) 4 (2017) 227.
[64] X. Dai, H. Cheng, Z. Bai, J. Li, Breast cancer cell line classification and its relevance with breast tumor subtyping, J. Cancer 8 (16) (2017) 3131.
[65] D.L. Holliday, V. Speirs, Choosing the right cell line for breast cancer research, Breast Cancer Res. 13 (4) (2011) 215.
[66] S. Loibl, L. Gianni, HER2-positive breast cancer, Lancet 389 (10087) (2017) 2415.
[67] A. Nasrazadani, R.A. Thomas, S. Oesterreich, A.V. Lee, Precision medicine in hormone receptor-positive breast cancer, Front. Oncol. 8 (2018) 144.
[68] L.T. Li, G. Jiang, Q. Chen, J.N. Zheng, Ki67 is a promising molecular target in the diagnosis of cancer (review), Mol. Med. Rep. 11 (3) (2015) 1566.
[69] Z. Inic, M. Zegarac, M. Inic, I. Markovic, Z. Kozomara, I. Djurisic, I. Inic, G. Pupic, S. Jancic, Difference between luminal A and luminal B subtypes according to Ki-67, tumor size, and progesterone receptor negativity providing prognostic information, Clin. Med. Insights Oncol. 8 (2014) 107.
[70] Z.H. Li, P.H. Hu, J.H. Tu, N.S. Yu, Luminal B breast cancer: patterns of recurrence and clinical outcome, Oncotarget 7 (40) (2016) 65024.
[71] S.E. Smith, P. Mellor, A.K. Ward, S. Kendall, M. McDonald, F.S. Vizeacoumar, F.J. Vizeacoumar, S. Napper, D.H. Anderson, Molecular characterization of breast cancer cell lines through multiple omic approaches, Breast Cancer Res. 19 (1) (2017) 65.
[72] G. Bianchini, J.M. Balko, I.A. Mayer, M.E. Sanders, L. Gianni, Triple-negative breast cancer: challenges and opportunities of a heterogeneous disease, Nat. Rev. Clin. Oncol. 13 (11) (2016) 674.
[73] K. Dias, A. Dvorkin-Gheva, R.M. Hallett, Y. Wu, J. Hassell, G.R. Pond, M. Levine, T. Whelan, A.L. Bane, Claudin-low breast cancer; clinical & pathological characteristics, PLoS One 12 (1) (2017) e0168669.
[74] S. Badve, D.J. Dabbs, S.J. Schnitt, F.L. Baehner, T. Decker, V. Eusebi, S.B. Fox, S. Ichihara, J. Jacquemier, S.R. Lakhani, et al., Basal-like and triple-negative breast cancers: a critical review with an emphasis on the implications for pathologists and oncologists, Mod. Pathol. 24 (2) (2011) 157.
[75] E.A. Rakha, I.O. Ellis, Triple-negative/basal-like breast cancer: review, Pathology 41 (1) (2009) 40.
[76] A.A. Jitariu, A.M. Cimpean, D. Ribatti, M. Raica, Triple negative breast cancer: the kiss of death, Oncotarget 8 (28) (2017) 46652.
[77] K.A. Egland, X.F. Liu, S. Squires, S. Nagata, Y.G. Man, T.K. Bera, M. Onda, J.J. Vincent, R.L. Strausberg, B. Lee, et al., High expression of a cytokeratin-associated protein in many cancers, Proc. Natl. Acad. Sci. USA 103 (15) (2006) 5929.
[78] S.A. Joosse, J. Hannemann, J. Spotter, A. Bauche, A. Andreas, V. Muller, K. Pantel, Changes in keratin expression during metastatic progression of breast cancer: impact on the detection of circulating tumor cells, Clin. Cancer Res. 18 (4) (2012) 993.
[79] N.T. Ueno, J.R. Espinosa Fernandez, M. Cristofanilli, B. Overmoyer, D. Rea, F. Berdichevski, M. El-Shinawi, J. Bellon, H.T. Le-Petross, A. Lucci, et al., International consensus on the clinical management of inflammatory breast cancer from the Morgan welch inflammatory breast cancer research program 10th anniversary conference, J. Cancer 9 (8) (2018) 1437.
[80] M. Brentnall, L. Rodriguez-Menocal, R.L. De Guevara, E. Cepero, L.H. Boise, Caspase-9, caspase-3 and caspase-7 have distinct roles during intrinsic apoptosis, BMC Cell Biol. 14 (2013) 32.
[81] J. Morales, L. Li, F.J. Fattah, Y. Dong, E.A. Bey, M. Patel, J. Gao, D.A. Boothman, Review of poly (ADP-ribose) polymerase (PARP) mechanisms of action and rationale for targeting in cancer and other diseases, Crit. Rev. Eukaryot. Gene Expr. 24 (1) (2014) 15.